A&A 415, 1177–1185 (2004)
DOI: 10.1051/0004-6361:20034629


Astronomy & Astrophysics

# Radial mixing in protoplanetary accretion disks

## VI. Mixing by large-scale radial flows

Ch. Keller and H.-P. Gail

Institut für Theoretische Astrophysik, Universität Heidelberg, Tiergartenstraße 15, 69121 Heidelberg, Germany

Received 20 March 2003 / Accepted 21 November 2003

**Abstract.** The presence of crystalline dust materials in the outer, cold regions of protoplanetary accretion discs requires conditions for their formation, which are typical for the inner, warm regions of the disc. This suggests the existence of a mechanism that allows an efficient, outward-directed radial transport of material in accretion discs. Higher order analytical calculations, as well as numerical simulations reveal meridional flow structures in $\alpha$-discs, which exhibit outflow of matter in regions near the disc midplane and may play a significant role in radial mixing in protoplanetary accretion discs. We present an analytical, isothermal model for the large-scale meridional flow pattern in an $\alpha$-disc, verifying the approximations which it is based on by means of a 2-D numerical computation. The solution for the flow structure obtained is used for calculating the transport of a tracer in accretion discs in combination with diffusional mixing. The impact of radial flows on mixing of tracers is compared to the height-averaged inflow solution of the standard one-zone approximation.

**Key words.** accretion disks – dust – solar system: formation – hydrodynamics

## 1. Introduction

Observations of silicate bands in cometary material (e.g. Hanner et al. 1994; Wooden et al. 1999, 2000) suggest the existence of crystalline material in the cold outer regions of protoplanetary accretion discs (Bouwman et al. 2000). Since there is no indication of the presence of crystalline silicate dust in the interstellar medium, its origin is likely to be in the protoplanetary disc itself. The processing of amorphous dust into crystalline silicates requires temperatures of above 800 K, which are encountered in the inner parts of protoplanetary discs ($r \lesssim 1 \ldots 2$ AU), but not in regions beyond the Jupiter orbit, where comets are thought to form (Gail 2001; Wehrstedt & Gail 2002, henceforth called Papers I and II, respectively). Therefore radial transport of processed material from the warm inner to the cold outer regions of the protostellar discs has been suggested (Nuth 1999; Nuth et al. 2000).

Similarly, polyaromatic hydrocarbons, which occur in outer, cold regions of protostellar discs (e.g. Meeus et al. 2001) also need high temperatures and pressures typical for inner regions (Nuth & Hill 2000). Prebiotic molecules processed in the inner regions of the disc may have been transported beyond the ice-zone to be incorporated into comets and delivered to the Earth to allow the evolution of life (Hill et al. 2002).

*Send offprint requests to*: Ch. Keller,
e-mail: ckeller@ita.uni-heidelberg.de

Radial mixing processes by turbulent diffusion and annealing of amorphous dust have already been treated in our previous papers (Papers I and II) and by Bockelée-Morvan et al. (2002). These model calculations showed that mixing of annealed dust by turbulent diffusion from warm inner into cool outer disc regions can explain the observed fraction of crystalline dust in cometary nuclei.

Since the introduction of the one-zone approximation model, which describes geometrically thin, optically thick, turbulent accretion discs by averaging the vertical dependencies of the primary variables and solving the resulting radial disc equations (e.g. Shakura & Sunyaev 1973; Pringle 1981), several authors have pointed out the existence of large-scale meridional flows (Urpin 1984; Siemiginowska 1988; Kley & Lin 1992; Różyczka et al. 1994; Kluźniak & Kita 2000; Regev & Gitelman 2002) in their solutions of $\alpha$-discs. These flows are absent from models with height averaged radial drift resulting from the one-zone approximation.

The flows resulting from the one-zone approximation are directed inwards throughout the disc, whereas the large-scale meridional flows imply the occurrence of mass outflow in regions close to the disc midplane, where matter gets transported from the inner to the outer disc regions, and inflow in regions high above the midplane, dominating the overall mass transport in the accretion disc. The authors observe this phenomenon in a large variety of disc models and using different analytical, semi-analytical and numerical methods, derive their

solutions. However, since the flow-structures of numerical models are limited by their finite computational domain, it is their close agreement with analytical solutions that confirms the existence of large-scale flow structures, independent of artificial in- and outflow boundary conditions needed in numerical simulations. This suggests that large-scale flows may be of great importance to the radial mixing in protostellar discs.

The present paper is a first attempt to investigate the impact of large-scale flows on the radial mixing of tracers in protoplanetary accretion discs in combination with turbulent mixing. In Sect. 2, we therefore introduce a simple, isothermal disc model that takes into account higher order terms in the radial velocity equation and results in outflow of matter in the disc midplane for a large parameter range. The flow structure is then compared to a numerical test calculation including all terms of the governing equations, justifying the approximations made in the analytical solution. The resulting analytical expressions for the velocity components are used in Sect. 3 to solve the tracer equation that describes the mixing of tracers in a model disc, and to investigate the differences in the results produced by those models taking into account large-scale meridional flows and those which only consider height-averaged, radial accretion flows. The results will be discussed in Sect. 4.

## 2. Radial flows in accretion discs

### 2.1. An analytical model

#### 2.1.1. Basic equations

The model equations are written in axisymmetric, cylindrical coordinates, where the independent spatial coordinates of the position vector are the radius $r$ and the vertical height $z$. The continuity equation, describing the conservation of mass, then reads in its differential form

$$\partial_t \rho + \partial_z \rho v_z + \frac{1}{r}\partial_r r \rho v_r = 0. \tag{1}$$

Here, $v_z$ and $v_r$ denote the velocity components in vertical and radial direction, $\rho$ is the gas density and $\partial_x$ represents the partial derivative with respect to an independent variable $x$. After applying Eq. (1) to the equations that state the conservation of momentum (e.g. Landau & Lifshitz 1959), we obtain for the vertical velocity component the expression

$$\begin{aligned}\partial_t v_z + v_z\partial_z v_z + v_r\partial_r v_z = \\ -\frac{1}{\rho}\partial_z P - \partial_z\Phi + \frac{1}{\rho}\left(\frac{4}{3}\partial_z(\mu\partial_z v_z) + \frac{1}{r}\partial_r(\mu r\partial_r v_z)\right. \\ \left. -\frac{2}{3r}\partial_z(\mu\partial_r(r v_r)) + \frac{1}{r}\partial_r(\mu r\partial_z v_r)\right),\end{aligned} \tag{2}$$

for the radial velocity component

$$\begin{aligned}\partial_t v_r + v_z\partial_z v_r + v_r\partial_r v_r = \\ \frac{v_\phi^2}{r} - \frac{1}{\rho}\partial_r P - \partial_r\Phi + \frac{1}{\rho}\left(\partial_z(\mu\partial_z v_r) + \frac{4}{3r}\partial_r(\mu r\partial_r v_r)\right. \\ -\frac{2}{3r}\partial_r(\mu v_r) + \frac{2\mu}{3r^2}\partial_r(r v_r) - \frac{\mu}{r^2}v_r + \partial_z(\mu\partial_r v_z) \\ \left. -\frac{2}{3r}\partial_r(\mu r\partial_z v_z) + \frac{2\mu}{3r}\partial_z v_z\right),\end{aligned} \tag{3}$$

and for the specific angular momentum

$$\begin{aligned}\partial_t v_\phi r + v_z\partial_z v_\phi r + v_r\partial_r v_\phi r = \\ \frac{r}{\rho}\partial_z\mu\partial_z v_\phi + \frac{1}{\rho r}\partial_r r^3\mu\partial_r\frac{v_\phi}{r},\end{aligned} \tag{4}$$

where $v_\phi$ is the azimuthal velocity component, $\Phi$ the gravitational potential, $\mu \equiv \rho\nu$ the viscosity coefficient, and $P$ the gas pressure. This system of equations is closed by the ideal gas equation of state

$$P = c_s^2\rho. \tag{5}$$

In case of turbulent flows these equations are averaged according to principles described in McComb (1994). In lowest order the same equations are recovered with an empirical recipe to calculate the turbulent viscosity. For accretion discs it is standard practice to use the $\alpha$-description for the turbulent viscosity

$$\nu = \alpha H c_s, \tag{6}$$

according to Shakura & Sunyaev (1973). The isothermal sound speed is given by

$$c_s^2 = \frac{kT}{\mu_m m_H} \tag{7}$$

where $T$ is the gas temperature, $k$ is Boltzmann's constant, $\mu_m$ the mean molecular weight, and $m_H$ the proton mass.

The temperature $T$ and the isothermal sound velocity $c_s$ are assumed to be constant in the vertical direction. Model calculations in the 1+1 dimensional approximation show the temperatures to vary only slowly in the vertical direction, except near the outer boundary, where the temperature rapidly drops to the effective temperature of the disc surface (Ruden & Lin 1986).

We also assume the validity of the thin-disc approximation (e.g. Pringle 1981), i.e. $\frac{H}{r} \sim \epsilon$, where $H(r)$ is the disc height at a given radius $r$, which is given by

$$H(r) = \frac{c_s}{\Omega_K}, \tag{8}$$

and $\epsilon \ll 1$ (typically $\epsilon \approx 0.05 \ldots 0.1$). This is equivalent to the assumption $c_s \ll v_K$ for the isothermal sound speed and the Keplerian speed $v_K$.

In Sect. 2.1, we consider stationary solutions only and thus neglect temporal derivatives. In the following we derive approximate solutions for $v_\phi$ correct up to order $\epsilon^2$ and $v_r$ and $v_z$ up to order $\epsilon$.

### 2.1.2. The azimuthal velocity component

Neglecting terms of order higher than $\epsilon^2$, the stationary equation for the radial velocity component reduces to

$$0 = \frac{v_\phi^2}{r} - \frac{1}{\rho}\partial_\mathrm{r} P - \partial_\mathrm{r}\Phi + \frac{1}{\rho}\partial_z(\mu\partial_z v_\mathrm{r}). \tag{9}$$

Evolutionary timescales of protoplanetary accretion discs suggest a turbulent-viscosity parameter $\alpha$ in the range of $\alpha \lesssim 0.01$ (Ruden & Pollack 1991; Drouart et al. 1999; Calvet et al. 2000). We can therefore safely assume that $\alpha^2 < \epsilon$ and also neglect the viscous term in Eq. (9). If $\alpha$ exceeds some critical value $\alpha_\mathrm{c}$ this assumption might no longer be justified (Kley & Lin 1992; Kluźniak & Kita 2000; Regev & Gitelman 2002). The applicability of our models depending on $\alpha$ will be discussed in Sect. 4.

The gravitational force of a central potential exerted by a star of mass $M_\star$ is given by

$$\partial_\mathrm{r}\Phi = \frac{GM_\star}{r^2} - \frac{3}{2}\frac{GM_\star}{r^2}\left(\frac{z}{r}\right)^2, \tag{10}$$

accurate to terms of order $\epsilon^2$. Applying the Taylor expansion and the definition of the Keplerian speed

$$v_\mathrm{K} \equiv \sqrt{\frac{GM_\star}{r}},$$

Eq. (9) now becomes

$$v_\phi = v_\mathrm{K}\left(1 - \frac{3}{4}\left(\frac{z}{r}\right)^2 + \frac{r^2}{2GM_\star\rho}\partial_\mathrm{r} P\right) \tag{11}$$

in accord with Urpin (1984). Using the equation of state (5) we obtain

$$v_\phi = v_\mathrm{K}\left(1 - \frac{3}{4}\left(\frac{z}{r}\right)^2 + \left(\frac{1}{2}r\partial_\mathrm{r}\ln\rho + r\partial_\mathrm{r}\ln c_\mathrm{s}\right)\frac{H^2}{r^2}\right). \tag{12}$$

To further evaluate this expression, a model for the radial density and temperature distribution with an accuracy of the order of $\epsilon^0$ is required. We can thus resort to the solutions of the stationary one-zone approximation for the density (e.g. Pringle 1981)

$$\rho = \rho_\mathrm{c}\,\mathrm{e}^{-z^2/(2H^2)}. \tag{13}$$

The central density $\rho_\mathrm{c}$ in this model is given by

$$\rho_\mathrm{c} = \frac{\dot{M}_\mathrm{r}}{\alpha\sqrt{18\pi^3}}\frac{\Omega_\mathrm{K}^2}{c_\mathrm{s}^3}\left(1 - \sqrt{\frac{R_\star}{r}}\right), \tag{14}$$

where we used the definition $\Omega_\mathrm{K} \equiv v_\mathrm{K}/r$ of the Keplerian frequency, $R_\star$ the stellar radius, and $\dot{M}_\mathrm{r}$ the total radial mass accretion rate.

For the radial temperature distribution we assume a simple dependency given by

$$T(r) = T_{1\,\mathrm{AU}}\left(\frac{r}{1\,\mathrm{AU}}\right)^{-\lambda}, \tag{15}$$

where $\lambda$ is a free parameter and $T_{1\,\mathrm{AU}}$ equals the temperature at 1 AU. Vertically isothermal disc models with a temperature equal to the surface temperature correspond to $\lambda = \frac{3}{4}$. More complex models, including radiative diffusion approximation and dust opacities appropriate for protoplanetary discs, result in central temperature profiles that are close to $\lambda \approx 1$ in regions where ice-coated dust grains dominate the opacity and $\lambda \approx 0.62$ in regions where bare dust grains dominate the opacity (e.g. Wehrstedt & Gail 2003).

If only radii complying with $\frac{R_\star}{r} \lesssim \epsilon$ are being considered, Eq. (12) finally reduces to

$$v_\phi = v_\mathrm{K}\left(1 - \lambda_r\frac{c_\mathrm{s}^2}{v_\mathrm{K}^2} - \frac{1}{4}\lambda\frac{z^2}{r^2}\right), \tag{16}$$

with accuracy of order $\epsilon^2$, where

$$\lambda_\mathrm{r} \equiv \frac{1}{4}\left(6 - \lambda - \sqrt{\frac{R_\star}{r}}\right).$$

### 2.1.3. The radial velocity component

Equation (16) allows us to estimate vertical gradients containing the azimuthal velocity component $v_\phi$. The stationary angular momentum Eq. (4) to first-order accuracy can be written as

$$v_\mathrm{r} = \frac{2}{v_\mathrm{K}}\left(\frac{r}{\rho}\partial_z\mu\partial_z v_\phi + \frac{1}{\rho r}\partial_\mathrm{r} r^3\mu\partial_\mathrm{r}\frac{v_\phi}{r}\right), \tag{17}$$

in agreement with Urpin (1984). Siemiginowska (1988) and Różyczka et al. (1994, hereafter RBB), however, neglect the vertical derivative term in their analysis.

Making use of the temperature model (15) and results obtained in Sect. 2.1.2, Eq. (17) takes the form

$$v_r = \alpha\Big[3 - \tfrac{5}{2}\lambda - \tfrac{3}{2}f(r) - \frac{1}{2}(9 - 5\lambda)\left(\frac{z}{H}\right)^2\Big]\left(\frac{H}{r}\right)c_\mathrm{s}, \tag{18}$$

where

$$f(r) \equiv \left(\sqrt{\frac{r}{R_\star}} - 1\right)^{-1}.$$

Note that all terms in Eq. (18) are of the same order with respect to $\epsilon$.

In the midplane ($z = 0$) this solution for $v_\mathrm{r}(r, z)$ has the following property: for $r \to R_\star$ the term $-\frac{3}{2}f(r)$ becomes large and negative. Therefore, in the inner region $v_\mathrm{r}(r, 0) < 0$, which means an *inflow* of matter in the midplane of the disc. For $r \gg R_\star$ the term $-\frac{3}{2}f(r)$ approaches zero and $v_\mathrm{r}(r, 0) > 0$, provided $\lambda < \frac{6}{5}$. Thus, in the outer disc region $v_\mathrm{r}(r, 0) > 0$, which means an *outflow* in the midplane of the disc. There exists, then, a stagnation radius

$$\frac{r_\mathrm{stag}}{R_\star} = \left(\frac{9 - 5\lambda}{6 - 5\lambda}\right)^2, \tag{19}$$

defined by $v_\mathrm{r}(r_\mathrm{stag}, 0) = 0$.

In the disc region outside of the stagnation radius, the radial velocity component decreases with height $z$ until it vanishes at some point

$$z_0 = z_\lambda H: \quad z_\lambda := \sqrt{\frac{6 - 5\lambda - 3f(r)}{9 - 5\lambda}}. \tag{20}$$

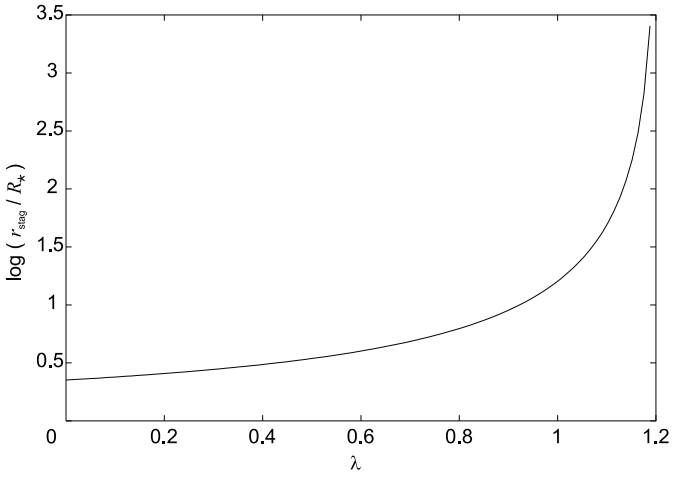


**Fig. 1.** The stagnation radius $r_{\rm stag}$ in units of the stellar radius $R_\star$ and as a function of the exponent $\lambda$ of the temperature power law $T \propto r^{-\lambda}$; $r_{\rm stag}$ diverges as $\lambda \to 1.2$. Outflows will only be observed for $\lambda < 1.2$.

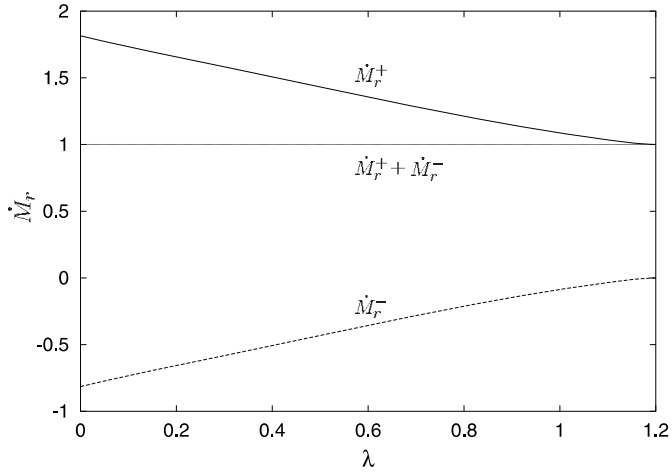


**Fig. 2.** In- and outflow rates $\dot{M}_{\rm r}^-$ and $\dot{M}_{\rm r}^+$ from the higher order approximation at large radii $r \gg R_\star$ in units of the mean accretion rate $\dot{M}_{\rm r}$, derived from standard one-zone disc models. The net mass flux rate is $\dot{M}_{\rm r}^- + \dot{M}_{\rm r}^+ = \dot{M}_{\rm r}$.

Hence, one has

$$v_{\rm r}(z) \begin{cases} >0 & \text{for } |z| < z_0 \\ =0 & \text{for } |z| = z_0 \\ <0 & \text{for } |z| > z_0. \end{cases} \tag{21}$$

The outward flow close to the midplane of the disc, thus, turns into an inwards flow in higher disc regions. A typical example for this flow is shown in Fig. 4.

In the disc region inside of the stagnation radius, the radial velocity component is directed inwards for all $z$. This result is independent of $\alpha$, contrary to the results obtained by Regev & Gitelman (2002), since we only consider small $\alpha^2 < \epsilon$ (Sect. 2.1.2).

In the limit of $\lambda \to \frac{6}{5}$ the stagnation point $r_{\rm stag}$ tends to infinity and we observe inflow throughout the disc if $\lambda \geq \frac{6}{5}$. The dependence of $r_{\rm stag}$ on $\lambda$ is shown in Fig. 1. For $\lambda = 1$ or $\lambda = \frac{3}{4}$ we find $r_{\rm stag} = 16\, R_\star$ or $r_{\rm stag} = 5.4\, R_\star$, respectively. The stagnation radius is therefore located well inside the region of dust vaporization in a protoplanetary accretion disc and at small radii, where the assumptions made leading to Eq. (16) might no longer apply.

As a result of this, there will be an outward transport of matter from hot disc regions, where dust is equilibrated, into cold outer disc regions, where equilibration is impossible.

Equation (18) can be compared to the solution for the inwards flow of the standard, height-averaged one-zone model (e.g. Pringle 1981)

$$\langle v_{\rm r} \rangle = -\frac{3}{2}\alpha \left(\frac{H}{r}\right) \frac{c_{\rm s}}{1 - \sqrt{\frac{R_\star}{r}}}, \tag{22}$$

which is shown in Fig. 5. Setting $\lambda = 1$, the ratio of the meridional radial flow structure $v_{\rm r}$ to the height-averaged inflow $\langle v_{\rm r} \rangle$ is

$$\frac{v_{\rm r}}{\langle v_{\rm r} \rangle} = -\frac{1}{3} + \frac{4}{3}\left(\frac{z}{H}\right)^2 + f(r). \tag{23}$$

For large radii, where $f(r) \to 0$ we obtain $v_{\rm r} = -\frac{1}{3}\langle v_{\rm r} \rangle$ in the disc midplane, which coincides with the numerical results of RBB, who have used Rosseland mean opacities appropriate for dust grains and molecules at temperatures $T < 3000$ K in their simulations including a flux-limited radiative diffusion equation.

**Table 1.** Numerical values of the in- and outflow rates for typical values of $\lambda$ and at large radii $r \gg R_\star$.

| $\lambda$ | 1 | 0.75 | 0.62 |
|---|---|---|---|
| $\dot{M}_{\rm r}^- / \dot{M}_{\rm r}$ | −0.087 | −0.250 | −0.344 |
| $\dot{M}_{\rm r}^+ / \dot{M}_{\rm r}$ | 1.087 | 1.250 | 1.344 |

### 2.1.4. Mass transport

By means of the error-function erf $\equiv \frac{2}{\sqrt{\pi}} \int_0^z \mathrm{e}^{-t^2}\, \mathrm{d}t$ and a symmetry condition with respect to the equatorial plane, we obtain for the mass outflow rate in the disc region $|z| < z_0$ close to the midplane

$$\begin{aligned} \dot{M}_{\rm r}^- &\equiv -2\pi r \int_{-z_0}^{+z_0} \rho v_{\rm r}\, \mathrm{d}z \\ &= \dot{M}_{\rm r} \left(1 - \sqrt{\frac{R_\star}{r}}\right) \left[ (1 + f(r)) \operatorname{erf}\left(\frac{z_\lambda}{\sqrt{2}}\right) \right. \\ &\quad \left. - \frac{2}{\sqrt{18\pi}} (9 - 5\lambda)\, z_\lambda\, \mathrm{e}^{-z_\lambda^2/2} \right]. \end{aligned} \tag{24}$$

As expected, the mass inflow rate in the higher disc regions $|z| > z_0$ becomes

$$\dot{M}_{\rm r}^+ := -2\pi r \cdot 2 \int_{z_0}^{\infty} \rho v_{\rm r}\, \mathrm{d}z = \dot{M}_{\rm r} - \dot{M}_{\rm r}^-, \tag{25}$$

which means that the net mass accretion rate $\dot{M}_{\rm r}$ is in accord with the result for the one-zone approximation. Expanding the error-function erf (e.g. Abramowitz & Stegun 1964), we obtain

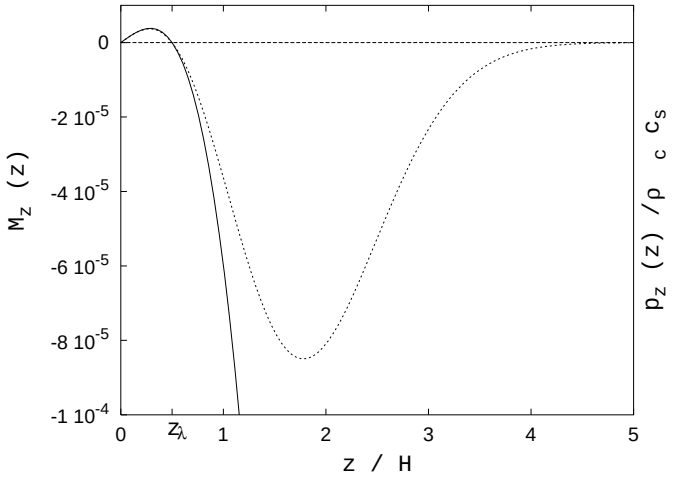


**Fig. 3.** Vertical profile of the momentum $p_z$ scaled by $\rho_c c_s$ (dashed line) and the Mach number $M_z$ (solid line) in vertical direction, for $\lambda = 1$ and large radii $r \gg R_\star (f(r) \to 0)$. The vertical flow is directed outwards close to the equator and changes sign at the same height as the radial velocity component.

an expression of the outflow rate at large radii $r \gg R_\star$ as a function of $\lambda$

$$\dot{M}_\mathrm{r}^-(\lambda) = \dot{M}_\mathrm{r} z_\lambda \sqrt{\frac{2}{\pi}} \left[ 1 - \frac{1}{3}\left(\frac{z_\lambda}{\sqrt{2}}\right)^2 + \frac{1}{10}\left(\frac{z_\lambda}{\sqrt{2}}\right)^4 - \frac{1}{42}\left(\frac{z_\lambda}{\sqrt{2}}\right)^6 - \frac{1}{3}(9-5\lambda)\mathrm{e}^{-z_\lambda^2/2} \right], \tag{26}$$

where $z_\lambda$ is defined in Eq. (20). This function along with the inflow rate $\dot{M}_\mathrm{r}^+(\lambda)$ is displayed in Fig. 2. The numerical values derived from Eq. (26) are listed in Table 1 for a set of typical values for $\lambda$: in the case of $\lambda = 1$, about 9% of the net mass flux rate are being carried outwards, 25% for $\lambda = \frac{3}{4}$ and 34% for $\lambda = 0.62$.

### 2.1.5. The vertical velocity component

In the stationary limit, the continuity Eq. (1) reads

$$\partial_z \rho v_z + \frac{1}{r}\partial_\mathrm{r} r \rho v_\mathrm{r} = 0. \tag{27}$$

This can be interpreted as an ordinary differential equation

$$\frac{\mathrm{d}p_z}{\mathrm{d}z} = R(z) \tag{28}$$

for the vertical momentum $p_z \equiv \rho v_z$ and a known r.h.s.

$$R(z) \equiv -\frac{1}{r}\partial_\mathrm{r} r \rho\, v_\mathrm{r}. \tag{29}$$

Applying the symmetry condition $p_z(z)|_{z=0} = 0$, Eq. (28) has the solution

$$p_z(z) = \int_0^z R(z')\,\mathrm{d}z'. \tag{30}$$

With the aid of the error-function, Eq. (30) can be integrated, which leads to the expression for the vertical velocity component

$$v_z(z) = \left[ A\frac{z}{H} + B\left(\frac{z}{H}\right)^3 \right] c_\mathrm{s}, \tag{31}$$

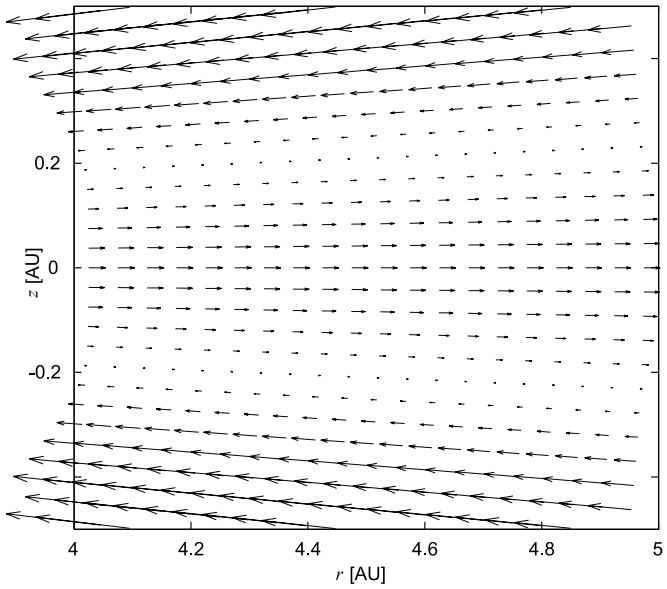


**Fig. 4.** Meridional flow pattern in the higher order approximation for the parameters $\lambda = 0.75$, $\alpha = 0.01$, $R_\star = 3.5\ R_\odot$, $M_\star = 1\ M_\odot$, $T(1\,\mathrm{AU}) = 1000$ K, $\dot{M}_\mathrm{r} = 10^{-7}\ M_\odot/\mathrm{yr}$.

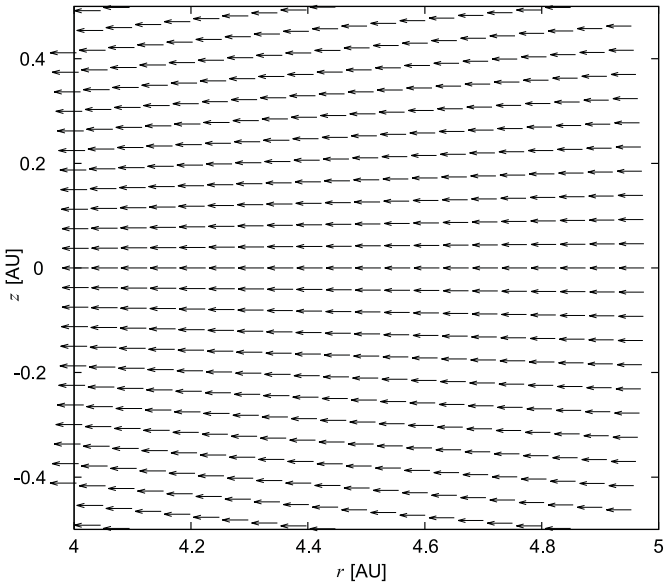


**Fig. 5.** Flow pattern of the standard, height-averaged one-zone approximation (cf. Fig. 4).

where

$$A \equiv \frac{\alpha}{4}\left(\frac{H}{r}\right)^2 \left[(3-\lambda)(6-5\lambda) - 2(9-4\lambda) f(r)\right],$$

$$B \equiv -\frac{\alpha}{4}\left(\frac{H}{r}\right)^2 (3-\lambda)(9-5\lambda).$$

The Mach number $M_z \equiv v_z/c_\mathrm{s}$ that results from the vertical velocity component $v_z$ is illustrated in Fig. 3 along with the vertical momentum component $p_z$ scaled by $\rho_c c_\mathrm{s}$. An example of the meridional flow pattern resulting from both velocity components $v_\mathrm{r}$ and $v_z$ is shown in Fig. 4, which compares to the flow structure of the height-averaged one-zone approximation shown in Fig. 5.

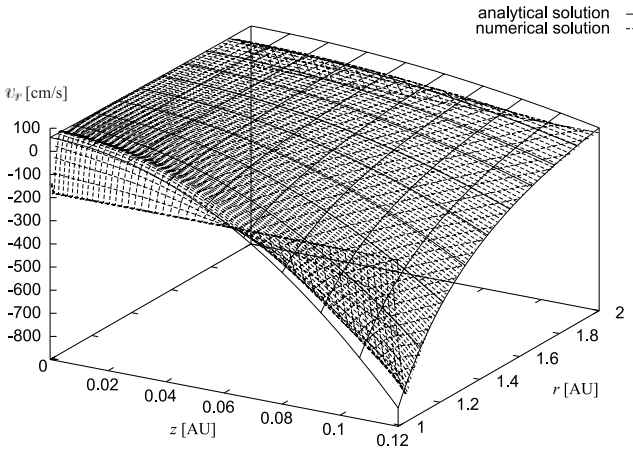


**Fig. 6.** The radial velocity component after relaxation in comparison to the analytical solution.

### 2.2. A numerical test

To verify the analytical approximations of Sect. 2.1, we compare the resulting flow structure with a numerical hydrodynamics simulation in spherical coordinates that includes all the terms in the governing equations of isothermal, axisymmetric flows. Since the full underlying Navier-Stokes equations in spherical coordinates are somewhat lengthy, we refer the reader to text books (e.g. Landau & Lifshitz 1959). The equations are solved in the vertically isothermal limit, therefore the four conservation equations for mass and momentum are closed by the equation of state (5) and the $\alpha$-description for the turbulent viscosity, Eq. (6).

The computations have been carried out on a staggered grid in spherical coordinates, using a finite volume discretization scheme described in detail by Stone & Norman (1992).

In a test calculation, the computational domain comprises an area of $r = 1$ to 2 AU and $\theta = 82$ to $90°$, which corresponds to a vertical height of about $z = 0.15$ AU at the inner and 0.3 AU at the outer boundary. The domain was resolved by $80\times60$ grid points.

We have used the following set of parameters: $\alpha = 10^{-2}$, $M_\star = 1\ M_\odot$, $\mu_\mathrm{m} = 7/3$, $T_{1\,\mathrm{AU}} = 10^3$ K, $\lambda = 1$, and $\dot{M}_\mathrm{r} = 10^{-6}\ M_\odot/\mathrm{yr}$.

Boundary conditions were derived from the stationary one-zone approximation, i.e. Dirichlet boundary conditions for the radial and angular velocity components at the inner and outer radii and von Neumann boundary conditions at the equatorial plane. For the poloidal velocity component, we have applied homogenous Dirichlet boundary conditions at the equatorial plane and homogenous von Neumann boundary conditions at the inner and outer boundary. At the upper boundary at $\theta = 82°$ we have used Dirichlet boundary conditions for all variables.

In the computation discussed here we have neglected terms involving $\sqrt{R_\star/r}$, which formally corresponds to a vanishing stellar radius and has no significant influence on the flow structure.

Figure 6 shows the numerical result of the radial velocity component after relaxation in comparison to the analytical solution. Apart from a thin zone of about 5 to 10 grid points along the boundaries, the analytical approximation and numerical solution of the fully coupled equations coincide well. This justifies the approximations introduced in determining the analytical solutions for $v_\phi$, $v_\mathrm{r}$ and $v_\mathrm{z}$.

## 3. Diffusion and transport of a tracer

The results of Sect. 2 show that the accretion flow in a disc is not simply an inwards drift of matter at all disc heights, but that under conditions prevailing in real discs ($\lambda \lesssim 1$) the net accretion rate results from a small but non-negligible outward transport of matter in the disc midplane and a dominating inward transport in higher disc layers. The outward transport of matter in the midplane has the consequence that some material from hot inner disc regions is brought into the cold outer disc regions, which again has consequences for the composition of the bodies formed in the outer parts of the disc, since then they contain some fraction of material which comes from inner disc regions.

In viscous accretion discs, where turbulence is the source of viscosity, this advective, outward-directed transport of material is superposed by turbulent diffusional transport of material between different disc regions. This also results in a transport of some fraction of matter from inner parts to the cold outer parts of the disc (e.g. Morfill 1983; Papers I and II and references therein).

Additionally, turbulent diffusional mixing, as well as, to a much lesser extent, advection, also acts in the vertical direction and mixes matter from the inner layers close to the midplane, where matter flows outwards towards outer radii, to higher levels, where matter flows inwards towards the central star. The vertical mixing tends to smooth out compositional differences due to the large-scale meridional flow. It is therefore important to study the combined effects of turbulent diffusion and meridional currents in two dimensions.

### 3.1. The model calculation

For this purpose, we numerically solve the time-dependent tracer equation

$$\partial_\mathrm{t}\, nc + \nabla\cdot nc\,\boldsymbol{v} = \nabla\cdot\frac{n\nu}{S_\mathrm{dg}}\nabla c \tag{32}$$

in axisymmetric, spherical coordinates in two dimensions, where $n$ represents the total particle density, $c$ the concentration, and $S_\mathrm{dg}$ the Schmidt number of a dust tracer of low density in the carrier gas. The Schmidt number is approximated by

$$S_\mathrm{dg} = 1$$

(see Papers I and II and references therein). The second term on the l.h.s. of the tracer Eq. (32) is the advection term that competes with the diffusive term on the right.

Ideally, Eq. (32), usually including additional gain and loss terms not considered here, needs to be solved for a set of dust species together with the fully coupled radiation hydrodynamics equations. This will be the subject of future work.

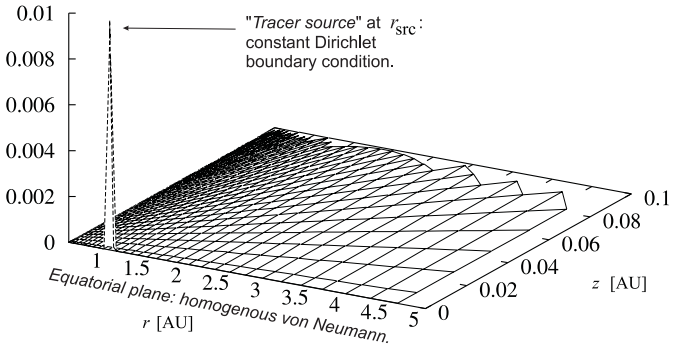


**Fig. 7.** Illustration of the implemented boundary conditions, designed to simulate the constant production of a tracer in the equatorial plane at 1 AU.

To gain first insight into the possible impact of large-scale flow structures on the transport of a dust tracer, we combine Eq. (32) with the stationary, analytical solutions for the flow-structure $\boldsymbol{v}(r, z)$, which we insert into the advection term. That way we can compare the qualitative differences between the result for the mean radial velocity (22) resulting from the standard one-zone approximation (SOZ) and the velocity field inferred from the higher order approximation (HOA) in Sect. 2.1, Eqs. (18) and (31).

For this computation we assume that the disc structure does not evolve. This is not strictly true (Wehrstedt & Gail 2003) but should be sufficiently accurate for the present type of explorative test calculations.

We solve Eq. (32) on a staggered, radial logarithmic grid of $100 \times 80$ grid points distributed over a domain spanning a radius from 0.1 to 200 AU and an angle from $\theta = 80$ to $90°$, using a fully implicit, backward Euler time-integration scheme.

To simulate the constant production of a dust tracer at a certain radius $r_{src}$ in the disc midplane, we have implemented a point source Dirichlet boundary condition for the primary variable ($nc$) at this position, whereas all other grid points along the equatorial boundary obey homogenous von Neumann boundary conditions. With a constant particle density $n$, this is equivalent to a constant concentration $c = 0.01$ at $r_{src}$ (Fig. 7). Furthermore, homogenous Dirichlet conditions have been applied to the inner and outer boundaries and a homogenous von Neumann condition at the upper boundary of our disc model.

### 3.2. Results

The results of the numerical computations for the vertically averaged surface concentration

$$C = \frac{2}{\int_{-\infty}^{\infty} n \mathrm{d}z} \int_0^{\infty} nc \, \mathrm{d}z \tag{33}$$

and for a set of fixed parameters (Table 2) are presented in Figs. 8–10. The tracer concentrations are plotted at different time levels, comparing the results of the models SOZ and HOA for the parameters $\lambda = 0.62$, $\lambda = 0.75$ and $\lambda = 1$.

Figure 8 shows the results for $\lambda = 1$. Neither at $t = 10^5$ yr, nor at $t = 10^6$ yr significant differences in the tracer distribution at large radii are noted. Diffusion dominates the tracer transport

**Table 2.** Set of fixed parameters used in the simulation of tracer transport in protostellar discs.

| $\alpha$ | $R_\star$ | $M_\star$ | $T_{1\,\mathrm{AU}}$ | $\dot{M}_\mathrm{r}$ | $S_\mathrm{dg}$ | $r_\mathrm{src}$ |
|---|---|---|---|---|---|---|
| 0.01 | $3.5\,R_\odot$ | $1\,M_\odot$ | $10^3$ K | $10^{-7}\,\frac{M_\odot}{\mathrm{yr}}$ | 1 | 1 AU |

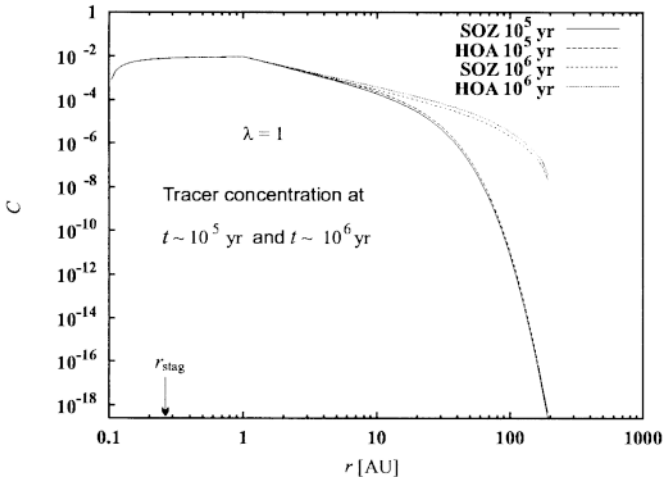


**Fig. 8.** Tracer concentrations $C$ for $\lambda = 1$ ($r_\mathrm{stag} \approx 0.26$ AU) at $t = 10^5$ yr and $t = 10^6$ yr. The results using the higher order approximation flow (HOA) hardly differs from the result of the standard one-zone approximation (SOZ).

to such an extent that the differences in the advective flows between the models SOZ and HOA become nearly negligible.

In Figs. 9 and 10 the results for $\lambda = 0.75$ are plotted for the time levels $t = 10^5$ yr and $t = 10^6$ yr, respectively. Here, the differences between the models become increasingly visible. Whereas at $t = 10^5$ yr, the surface concentration $C$ at $r = 100$ AU computed with the HOA model exceeds the result obtained with the SOZ by a factor of about 5, at $t = 10^6$ yr the HOA concentration $C \approx 4.3 \times 10^{-5}$ at 100 AU is about 13 times larger than the value $3.2 \times 10^{-6}$ of a SOZ calculation.

For $\lambda = 0.62$ the results of the HOA and the SOZ models differ the most. The tracer concentrations $C$ at $t = 10^6$ yr for each model is displayed in Fig. 11. At $r = 100$ AU, $C$ computed with the HOA model exceeds the result obtained with the SOZ by a factor of about 68.

Correspondingly, applying the flow structure of the HOA model, to reach a concentration of $C = 10^{-4}$ at 10 AU, for $\lambda = 0.75$ it only takes about a factor of 0.6 of the time required in the SOZ, i.e. $2.1 \times 10^4$ yr instead of $3.4 \times 10^4$ yr. For $\lambda = 0.62$ the time needed to reach $C = 10^{-4}$ at 20 AU is about a factor 0.5 shorter in the HOA model then in the SOZ model, i.e. $1.4 \times 10^4$ yr instead of $2.8 \times 10^4$ yr.

According to the model calculations, a temperature profile ($\lambda = 1$) corresponding to the central, radial temperature distribution with dust opacities adequate for ice-coated grains, which prevail in a large portion of protostellar discs, results in no significant difference between the tracer mixing obtained from the two models SOZ and HOA. This suggests that the tracer mixing in the SOZ in this case yields adequate results. On the other

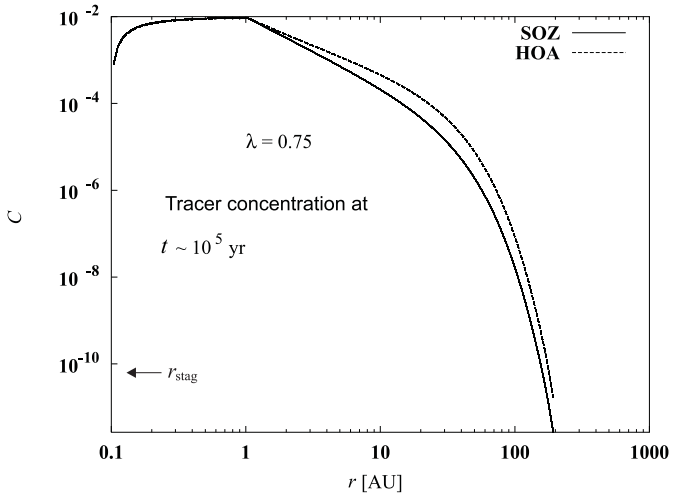


**Fig. 9.** Tracer concentrations $C$ for $\lambda = 0.75$ ($r_{\rm stag} \approx 0.09$ AU) at $t = 10^5$ yr. At 100 AU $C$ computed with the model using the HOA exceeds the result of the SOZ by a factor of about 14.

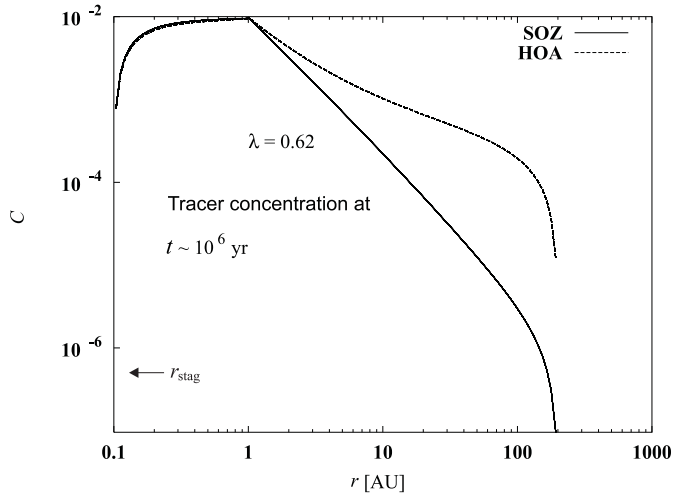


**Fig. 11.** Tracer concentrations $C$ for $\lambda = 0.62$ ($r_{\rm stag} \approx 0.07$ AU) at $t = 10^6$ yr. At 100 AU $C$ computed with the model using the HOA exceeds the result of the SOZ by a factor of about 63.

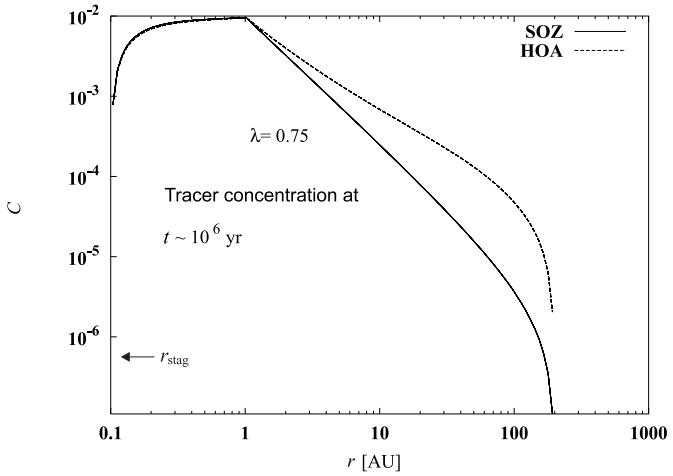


**Fig. 10.** Tracer concentrations for $\lambda = 0.75$ at $t = 10^6$ yr. At 100 AU $C$ computed with the model using the HOA exceeds the result of the SOZ by a factor of about 20.

hand, for a temperature profile appropriate for bare dust grains ($\lambda = 0.62$), the results for tracer mixing obtained from the SOZ and HOA models are significantly different from each other. This shows that much more sophisticated numerical models are necessary, before quantitative conclusions for the transport of tracers in large-scale disc flows can be drawn.

## 4. Discussion

The thin-disc approximation in the isothermal limit and the assumption of a sufficiently small value for the turbulent diffusion parameter $\alpha$ that allowed us to neglect the diffusive term in Eq. (9), results in the velocity field given by Eqs. (18) and (31), which shows an outflow in the equatorial plane for a large part of the disc, depending on the radial temperature profile given in Eq. (15).

Both velocity components are directly proportional to $\alpha$. Formally, in this model the velocity field retains its qualitative structure for any adequately small value of $\alpha$. Also, since for both models SOZ and HOA discussed in Sect. 3, the advection term and the diffusion term of the tracer Eq. (32) are proportional to $\alpha$, the same is true for the timescale of the mixing of a tracer, whereas the resulting differences when comparing the two models, are independent of $\alpha$.

In an analytical estimate, including the vertical diffusion term which we neglected in Eq. (9), Kley & Lin (1992) find a critical $\alpha_{\rm c}$ above which the disc flow is directed inwards for all heights $z$. For a disc around a white dwarf, they find $\alpha_{\rm c} \sim 0.06$, in good agreement with their simulation of a disc model comprising a region interior to 30 $R_\star$. Using the opacity parameters and equation of state taken from their protostellar disc model in the estimate of Kley & Lin (1992), RBB find a theoretical value of $\alpha_{\rm c} \sim 0.12$. Nevertheless, they do not observe a reversal of the equatorial outflow in their simulations even for values up to $\alpha = 0.25$.

In a semi-analytical computation including the Eddington approximation for the temperature distribution and electron scattering, respectively a Kramers opacity law, Regev & Gitelman (2002) obtain the stagnation radius $r_{\rm stag}$ as a function of $\alpha$. They define $\alpha_{\rm c}$ as the value, where $r_{\rm stag} \to \infty$ and find $\alpha_{\rm c} \gtrsim 0.7$ in good agreement with the analytical result obtained by Kluźniak & Kita (2000) using a polytropic equation of state. This critical value for $\alpha$ is undoubtedly drastically above the value one expects in protostellar discs. The authors conclude that the flow pattern is due to dynamical, rather than thermal processes. This is supported by our analysis, as well as the observation made by Regev & Gitelman (2002) that, while the disc structure depends somewhat on the opacity law, the meridional flow pattern and the stagnation radius are quite insensitive to it. We are therefore confident that, although we obtained our results from a rather crude thermal model describing the temperature profile in the disc, the flow pattern observed is real and of a universal nature.

However, if the value of $\alpha$ is reduced far enough, while radiative transport is also considered, RBB point out that the flow structure will be dominated by convective velocities. This is equivalent to a stability criterion given in Eq. (13) in their paper, originally investigated by Kley et al. (1993), where the Rayleigh number exceeds a critical value. Kley et al. (1993) find that instability occurs in their disc region for $\alpha = 10^{-3}$, but not for $\alpha = 10^{-2}$, consistent with the observations of RBB. For disc regions interior to 0.5 AU, RBB observe a dominating convection even with large values of $\alpha$.

Still, we do not expect convection in the inner disc regions to be a major restriction on the effect of equatorial outflow to the large-scale transport of tracers within discs. Tracers produced in the warm, inner regions can diffuse into regions, where the large-scale flow structures may dominate the velocity field and possibly also the mixing of tracers on their further journey into the ice zone of the outer parts of the disc.

All investigations on flow structures in accretion discs made in the present paper are based on the assumption that the viscosity can be approximated by the $\alpha$-prescription. There arises the delicate question to which extend the results of this and other model calculations depend on this particular assumption. This can only be checked by testing different recipies for treating the disc viscosity. Such calculations are currently underway, but we do not expect significant modifications.

Observations of cristalline silicates in comets (Wooden et al. 1999, 2000) and of cristallized material as part of the matrix material in primitive meteorites (e.g. Arrhenius & Asunmaa 1973) indicate large-scale radial mixing of disc material between hot inner and cool outer disc regions during the early stages of planetary system formation. Our calculations have shown that the radial mixing in protoplanetary discs is driven by two different physical mechanisms, by (i) turbulent mixing, which is already discussed by Morfill (1983), preceding papers in the present series and Bockelée-Morvan et al. (2002), and (ii) by large-scale meridional flows present in $\alpha$-discs, which are discussed in this paper. The large-scale flows support or even dominate the diffusive transport and need to be considered in future model calculations of mixing processes in accretion discs.

*Acknowledgements.* This work is part of a project of the special research project SFB 359 “Reactive Flows, Diffusion and Transport” which is supported by the Deutsche Forschungsgemeinschaft (DFG).

## References

Abramowitz, M., & Stegun, I. A. 1964, Handbook of Mathematical Functions (Toronto: General Publishing Company)
Arrhenius, G., & Asunmaa, S. K. 1973, The Moon, 8, 368
Bockelée-Morvan, D., Gautier, D., Hersant, F., Huré, J.-M., & Robert, F. 2002, A&A, 384, 1107
Bouwman, J., de Koter, A., van den Ancker, M. E., & Waters, L. B. F. M. 2000, A&A, 360, 213
Calvet, N., Hartmann, L. W., & Strom, S. E. 2000, in Protostars and Planets IV, ed. V. Mannings, A. P. Boss, & S. S. Russell (Tucson: University of Arizona Press), 377
Drouart, A., Dubrulle, B., Gautier, D., & Robert, F. 1999, Icarus, 140, 129
Gail, H.-P. 2001, A&A, 378, 192 (Paper I)
Hanner, M. S., Hackwell, J. A., Russel, R. W., & Lynch, D. K. 1994, Icarus, 112, 490
Hill, H. G. M., Grady, C. A., Nuth, J. A., & Heap, S. R. 2002, Lunar Planet Sci. Conf., 33, 1247
Kley, W., & Lin, D. N. C. 1992, ApJ, 397, 600
Kley, W., Papaloizou, J. C. B., & Lin, D. N. C. 1993, ApJ, 416, 679
Kluźniak, W., & Kita, D., 2000, preprint [astro-ph/0006266]
Landau, L. D., & Lifshitz, E. M. 1959, Fluid Mech. (Reading: Addison-Wesley)
McComb, W. D. 1994, The Physics of Fluid Turbulence (Oxford Clarendon Press)
Meeus, G., Waters, L. B. F. M., Bouwman, J., et al. 2001, A&A, 365, 476
Morfill, G. E. 1983, Icarus, 53, 41
Nuth, J. A. 1999, Lunar Planet Sci. Conf., 30, 1726
Nuth, J. A., & Hill, H. G. M. 2000, Lunar Planet Sci. Conf., 31, 1229
Nuth, J. A., Hill, H. G. M., & Kletetschka, G. 2000, Nature, 406, 275
Pringle, J. E., 1981, ARA&A, 19, 137
Regev, O., & Gitelman, L. 2002, A&A, 396, 623
Różyczka, M., Bodenheimer, P., & Bell, K. R. 1994, ApJ, 423, 736 (RBB)
Ruden, S. P., & Lin, D. N. C. 1986, ApJ, 308, 883
Ruden, S. P., & Pollack, J. B. 1991, ApJ, 375, 740
Shakura, N. I., & Sunyaev, R. A. 1973, A&A, 24, 337
Siemiginowska, A. 1988, Acta Astron., 38, 21
Stone, J. M., & Norman, M. L. 1992, ApJS, 80, 753
Urpin, V. A. 1984, SvA 28, 50
Wehrstedt, M., & Gail, H.-P. 2002, A&A, 385, 181 (Paper II)
Wehrstedt, M., & Gail, H.-P. 2003, submitted
Wooden, D. H., Harker, D. E., Woodward, C. E. et al. 1999, ApJ, 517, 1034
Wooden, D. H., Butner, H. M., Harker, D. E., & Woodward, C. E. 2000, Icarus, 143, 126